SCIENTIFIC REPORTS

OPEN

SUBJECT AREAS:
BATTERIES
ELECTRONIC PROPERTIES AND MATERIALS

Received
4 November 2013

Accepted
17 February 2014

Published
12 March 2014

Correspondence and requests for materials should be addressed to Y.-T.K. (yongtae@pusan.ac.kr)

Stabilization of Oxygen-deficient Structure for Conducting $Li_4Ti_5O_{12-\delta}$ by Molybdenum Doping in a Reducing Atmosphere

Hannah Song[1], Tae-Gyung Jeong[1], Young Hoon Moon[1], Ho-Hwan Chun[2], Kyung Yoon Chung[3], Hyung Sun Kim[3], Byung Won Cho[3] & Yong-Tae Kim[1]

[1]Department of Energy System, Pusan National University, Busan 609-735, Republic of Korea, [2]Global Core Research Center for Ships and Offshore Plants (GCRC-SOP), Pusan National University, Busan 609-735, Republic of Korea, [3]Center for Energy Conversion, Korea Institute of Science and Technology, Seoul 130-650, Korea.

$Li_4Ti_5O_{12}$ (LTO) is recognized as being one of the most promising anode materials for high power Li ion batteries; however, its insulating nature is a major drawback. In recent years, a simple thermal treatment carried out in a reducing atmosphere has been shown to generate oxygen vacancies (V_O) for increasing the electronic conductivity of this material. Such structural defects, however, lead to re-oxidization over time, causing serious deterioration in anode performance. Herein, we report a unique approach to increasing the electronic conductivity with simultaneous improvement in structural stability. Doping of LTO with Mo in a reducing atmosphere resulted in extra charges at Ti sites caused by charge compensation by the homogeneously distributed Mo^{6+} ions, being delocalized over the entire lattice, with fewer oxygen vacancies (V_O) generated. Using this simple method, a marked increase in electronic conductivity was achieved, in addition to an extremely high rate capability, with no performance deterioration over time.

$Li_4Ti_5O_{12}$ (LTO) with a cubic spinel structure has demonstrated outstanding cyclability and safety when used as the anode material of high power Li ion batteries. This is due to their zero-strain properties, which give a long cycle life, and to their relatively high potential range (1.5 V vs Li^+/Li) in the charge/discharge process, which results in no dendrite formation[1–3]. Owing to these attributes, LTO is considered to be the most promising alternative anode material to conventional graphitic materials; however, its inherent low electronic conductivity ($<10^{-13}$ S cm^{-1})[4] needs to be enhanced in order to increase the rate capability. For this purpose, several approaches have been developed such as the preparation of nanoscale LTO[5,6], forming a composite with conducting materials[7,8], and doping with various metals[9,10]. Alternatively, it was recently reported that the generation of oxygen vacancies (V_O) can induce partial reduction of Ti sites in the LTO lattice on thermal treatment in a reducing atmosphere. The reaction can be described using Kroger-Vink notation as $O_0^x = 1/2O_2(g) + V_0^{k\bullet} + ke'$ (k = 0, 1, 2)[11]. This resulted in enhanced rate capability due to the marked increase in electronic conductivity[12–14]. This approach is believed to be a highly cheap and efficient method from an engineering viewpoint, in comparison with the abovementioned methods, because the electronic conductivity can be readily increased up to 10^{-7} S cm^{-1} by using a simple thermal treatment process in a reducing atmosphere. Unfortunately, this approach has two serious drawbacks, primarily caused by the oxygen vacancy generation. The first of these is that because the partially reduced state of Ti in the LTO lattice is unstable in air, re-oxidization into the original Ti^{4+} state readily occurs and therefore the high conductivity gradually diminishes over time[15,16]. The second issue is that the oxygen vacancies (V_O) generated by partial reduction can lead to lattice distortion and ultimately a decrease in Li ion mobility in the LTO lattice[17].

In the present study, we have designed an LTO material that has markedly higher electronic conductivity, but without the issues associated with oxygen vacancy generation. As the oxygen vacancies (V_O) were generated by charge compensation for the reduced Ti^{4+} ions in a reducing atmosphere, we attempted to partially reduce Ti^{4+} ions in 16 d sites with dopants having higher valences such as 5+ or 6+, instead of generating oxygen vacancies (V_O). Among the various transition metals that could potentially be used for achieving this, we selected Mo as a

dopant. It is widely recognized that this metal can readily maintain a 6+ valence state in a reducing atmosphere (10% H_2, 90% Ar) up to 800°C, with a spinel structure being easy to form via solid state reaction of precursors, in addition to having an adequate ionic radius for replacing Ti^{4+} ions in the lattice[18]. It was revealed that the Mo-doped LTO prepared in a reducing atmosphere resulted in a marked increase in electronic conductivity (10^{-2} S cm^{-1}), which was over 10 orders of magnitude higher than that of bare LTO. Furthermore, an excellent capacity at a high C-rate (167 mAh g^{-1} at 10 C) was achieved, which is close to the theoretical value (172 mAh g^{-1} for 3% Mo-doped LTO). To the best of our knowledge, the value obtained in the present study is the highest among the reported values for doped LTO samples in the literature.

Results

Four different materials were prepared, LTO-O (undoped LTO in an oxidizing atmosphere), LTO-R (undoped LTO in a reducing atmosphere), Mo-LTO-O (Mo-doped LTO in an oxidizing atmosphere), and Mo-LTO-R (Mo-doped LTO in a reducing atmosphere). Figure 1 shows the X-ray diffraction patterns obtained for the four materials. It can be clearly seen that all the samples except for Mo-LTO-O were successfully prepared in a single phase without any trace of byproducts. However, for the Mo-LTO-O, a byproduct phase corresponding to Li_2MoO_4 is evident, implying that in oxidizing conditions, Mo ions cannot efficiently replace the Ti^{4+} sites in the lattice. This might be because Li_2MoO_4 is readily formed by the reaction of Li_2CO_3 and MoO_3 below the thermal treatment temperature of 800°C. In addition, the size of the Mo-LTO-O particles was found to be in the range of a few micrometers, which is significantly different from that of the few hundreds of nanometers of the other samples (Figure S1), indicating that the Mo doping did not occur effectively in the oxidizing atmosphere. Hence, no further investigation was carried out on the Mo-LTO-O samples in this study. As the lattice parameter (8.360(1) Å) obtained from the Rietveld refinement was the same for the three remaining samples (Table S1), the effect of the Mo dopant or preparation atmosphere on the lattice size and Li ion conduction path can be disregarded. On the other hand, the colors of the different samples were distinct, as shown in the inset of Figure 1. As the colors of LTO-R and Mo-LTO-R were much darker than that of the LTO-O, it was expected that their electronic conductivities would be significantly greater due to a reduction in the band gap.

Electronic conductivity enhancement can be directly measured with the 4-probe van der Pauw method, with which the two main components that affect electronic conductivity (electron mobility and carrier density) can be distinguished by measuring the Hall coefficient. Table 1 shows the electronic properties of the three materials. The electronic conductivity of LTO-O could not be measured with the employed system because its extremely low conductivity ($<10^{-13}$ S cm^{-1})[4] was out of the measurement range. The use of a reducing atmosphere resulted in efficient conductivity improvement, with the value for LTO-R being 8.1E−6 S cm^{-1}, which was similar to a previously reported value[12]. Mo doping in a reducing atmosphere had a remarkable effect on the conductivity, increasing to a value in the region of 10^{-2} S cm^{-1}, which is over 10 orders of magnitude higher than that of LTO-O, and 4 orders of magnitude higher than that of LTO-R. This remarkable conductivity enhancement can be attributed to an increase in carrier density rather than in electron mobility (Table 1), indicating that the Mo doping in the reducing atmosphere was n-type, and that extra charges were generated by the charge compensation process due to the higher valence of the Mo dopant. The difference in electronic conductivity was also clearly identified by measuring the band gaps using UV-vis spectroscopy, as shown in Figure S2. The band gap energies were measured to be 2.17, 0.99, and 0.22 eV for LTO-O, LTO-R, and Mo-LTO-R, respectively.

It is interesting to note that the conductivity improvement for LTO-R became negligible within a few weeks. As shown in

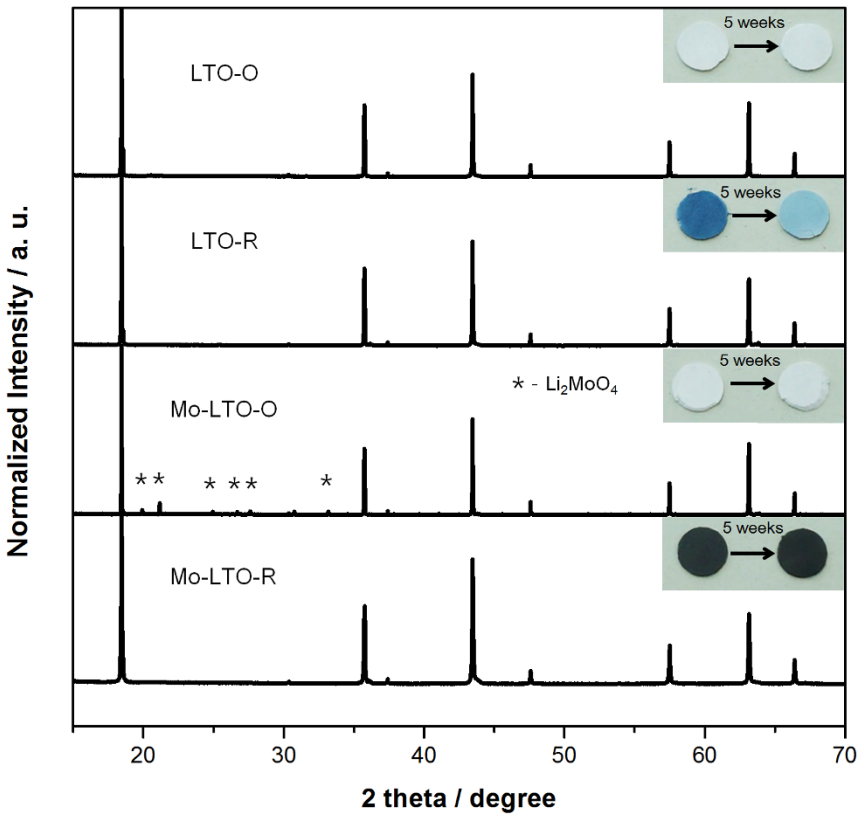

Figure 1 | HRPD patterns and colors of all samples.

Table 1 | Electronic conductivities, mobilities, and carrier densities of LTO-O, LTO-R, and Mo-LTO-R

Sample	Conductivity/S cm^{-1}	Mobility/$m^2V^{-1}s^{-1}$	Carrier density/m^{-3}
LTO-O (initial)		Not measured	
LTO-O (5 weeks later)		Not measured	
LTO-R (initial)	8.1E-6	4.5E0	1.1E + 13
LTO-R (5 weeks later)		Not measured	
Mo-LTO-R (initial)	1.1E-2	2.7E0	2.5E + 16
Mo-LTO-R (5 weeks later)	1.4E-2	4.5E0	1.9E + 16

Figure 1, the dark color of the LTO-R became lighter after 5 weeks in ambient conditions, indicating that the band gap was widened, resulting in a decrease in electronic conductivity. This may be because the structure of the LTO-R, which contained a number of oxygen vacancies (V_O), was unstable in the presence of air, causing the reduced Ti^{3+} ions to be oxidized into the stable Ti^{4+} state over time. Indeed, this re-oxidization phenomenon was clearly identified from the difference in electronic conductivity between the as-prepared material and that after storage for 5 weeks. As shown in Table 1, even though the electronic conductivity (8.1E−6 S cm^{-1}) of LTO-R measured directly after synthesis was about 7 orders of magnitude higher than LTO-O (<1.0E−13 S cm^{-1}), that after 5 weeks was below the measurement limit of the system. On the other hand, in the case of Mo-LTO-R, no color or electronic conductivity change was exhibited after 5 weeks in the same storage conditions. Hence, it is clear that in contrast to LTO-R, the structure of Mo-LTO-R was highly stable in air, indicating that fewer oxygen vacancies (V_O) were generated.

As the outstanding structural stability of Mo-LTO-R in air is likely to be related to a change in electronic structure and oxygen defect concentration caused by Mo doping, we carried out X-ray photoelectron spectroscopy (XPS) and electron paramagnetic resonance (EPR) analyses to gain further understanding of the origin of the enhanced stability. Figure 2 (a) shows the Ti 2*p* core level XPS spectra for LTO-O, LTO-R, and Mo-LTO-R measured directly after synthesis. In the case of LTO-O, a clear single peak set (Ti $2p_{1/2}$ and

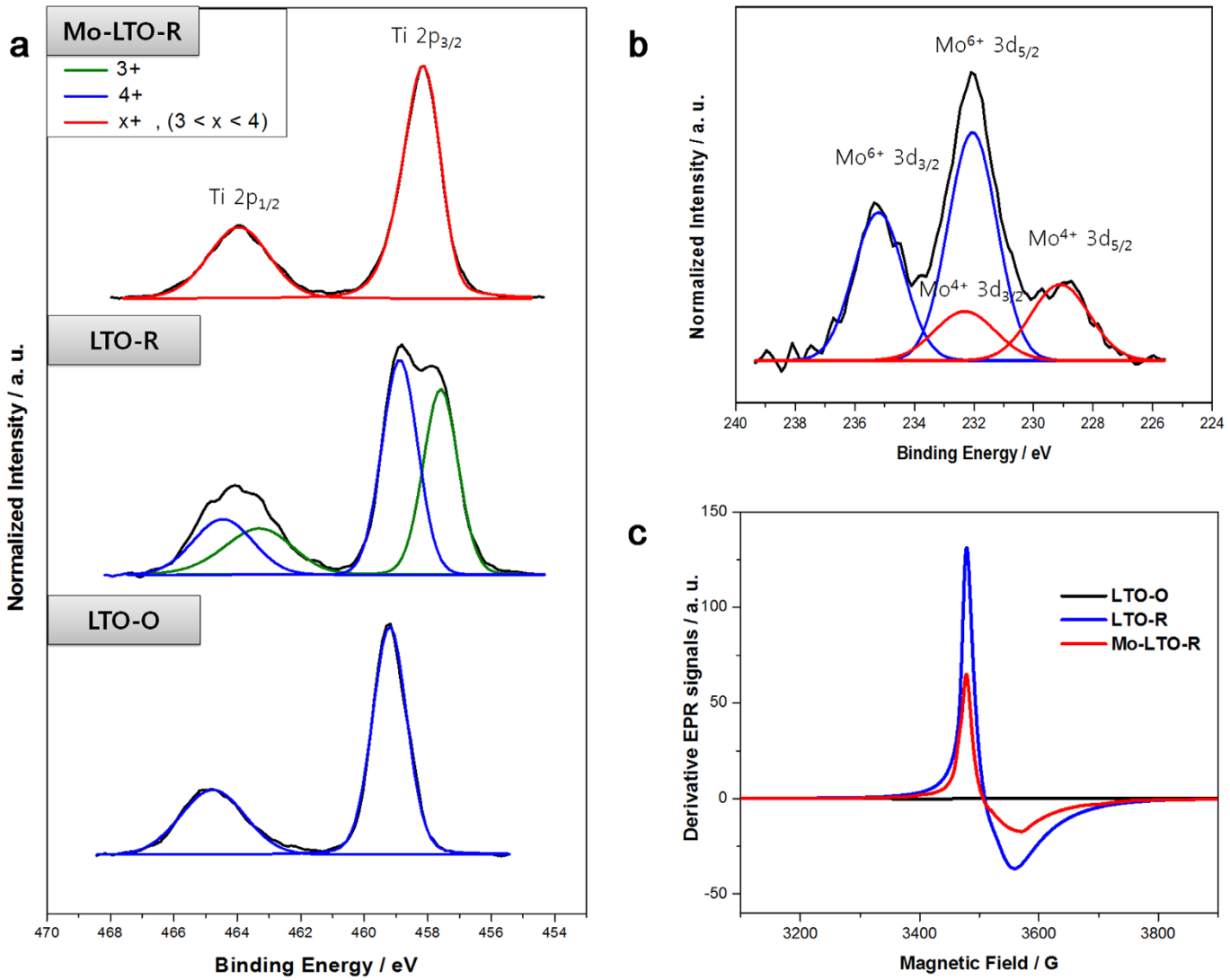

Figure 2 | (a) Ti 2p core-level XPS spectra of LTO-O, LTO-R, and Mo-LTO-R. (b) Mo 3 d XPS spectrum of Mo-LTO-R. (c) EPR signals of the three materials.

$2p_{3/2}$) corresponding to the Ti^{4+} state can be observed, with the peak position shifted to a slightly higher binding energy from the reference value because of the well-known final state effect due to their insulating nature[19]. The XPS spectrum for LTO-R, however, shows significantly different characteristics to that for LTO-O, with two split peak sets evident, which correspond to the Ti^{3+} and Ti^{4+} states. This indicates that approximately 45% of Ti^{4+} ions were reduced to the Ti^{3+} state by the generation of oxygen vacancies (V_O) in the reducing atmosphere. On the other hand, it is interesting to note that for Mo-LTO-R, a single peak set without any splitting can be seen, despite it having been prepared under the same conditions as for the LTO-R, and the binding energy was intermediate between those of the Ti^{3+} and Ti^{4+} states. It is widely recognized that a valence-averaged XPS peak at an intermediate binding energy can be obtained, as electron delocalization means that there is no locally discrete oxidation state[20,21]. Hence, this strongly suggests that Mo doping in the reducing atmosphere led to the partial reduction of Ti^{4+} ions, similar to that of LTO-R; however, it simultaneously led to electron delocalization over the entire lattice, which is clearly different from the locally discrete oxidation state caused by the spatially random generation of oxygen vacancies (V_O) in LTO-R. The charge compensation mechanism for the partial reduction of Ti^{4+} ions is therefore different for LTO-R (oxygen vacancy generation) and Mo-LTO-R (high valence of Mo dopant) in the reducing atmosphere.

Clear evidence for charge compensation by the high valence Mo dopant was provided by the XPS spectra of the Mo 3 d core level. As shown in Figure 2 (b), it can be clearly seen that the Mo dopant was in its Mo^{6+} rather than Mo^{4+} state (intensity ratio $Mo^{4+}:Mo^{6+} = 28:72$), confirming that the partial reduction of Ti^{4+} ions was caused by the charge compensation by the high valence Mo dopant, similar to n-type doping, rather than generation of oxygen vacancies (V_O) in the reducing atmosphere.

The expected decrease in oxygen vacancies (V_O) in Mo-LTO-R was verified using EPR spectroscopy, which is known to be a powerful tool for determining the concentration of oxygen vacancies (V_O) based on the paramagnetic nature of Ti^{3+} ions in the vicinity of oxygen vacancies (V_O)[22,23]. As shown in Figure 2 (c), while no EPR signal was detected for LTO-O, as Ti^{4+} has no unpaired electrons with paramagnetic nature, for the LTO-R, there was a strong signal at a g-value of 1.99, corresponding to the Ti^{3+} state, verifying the high concentration of oxygen vacancies (V_O). In the case of Mo-LTO-R, however, the signal was markedly lower than that observed for the LTO-R, indicating fewer oxygen vacancies (V_O). This was because, as confirmed by the XPS results, the partial reduction of Ti^{4+} ions occurred not due to oxygen vacancy generation leading to a locally discrete valence state, but by charge compensation by the high valence Mo dopant followed by electron delocalization over the entire lattice in the reducing atmosphere. In summary, based on the XPS and EPR studies, it appears that Mo doping in the reducing atmosphere led to the increase in electronic conductivity through partial reduction of Ti^{4+} ions, and simultaneously led to an enhancement in structural stability through a decrease in the generation of oxygen vacancies (V_O) with electron delocalization. Thermal treatment in the reducing atmosphere resulted in an increase in electronic conductivity similar to that achieved by Mo doping, but it was impossible to secure structural stability, owing to the inevitable generation of oxygen vacancies (V_O).

As well as the problems associated with structural stability, the generation of oxygen vacancies (V_O) through thermal treatment in a reducing atmosphere can cause disadvantageous distortion of the Ti-centered octahedral (TiO_6) structure, leading to a change in Li ion mobility[9]. Thus, in order to investigate the fine structural changes in the three materials, we conducted X-ray absorption near edge structure (XANES) and extended X-ray absorbance fine structure (EXAFS) analyses using a synchrotron beam. Figure 3 (a) shows the Ti *K*-edge XANES spectra for LTO-O, LTO-R, and Mo-LTO-R. The pre-edge peak at around 4970 eV formed by the pure electric quadrupole 1 $s \rightarrow 3\ d$ transition under the hybridization of the Ti 3*d*–4*p* orbitals provides information on the local fine structure[24]. It can be seen that the pre-edge peak intensity for LTO-R was higher than that for LTO-O. This implies that the distortion of the TiO_6 octahedral structure for LTO-R was increased in comparison with LTO-O, as the increase of the pre-edge peak is directly related to a break in centrosymmetry, i.e., an increase in local distortion of the M–O octahedra leading to *p*–*d* orbital mixing[24,25]. On the other hand, because the pre-edge peak intensity for Mo-LTO-R was similar to that for LTO-O, it is clear that the structural distortion in the Mo-LTO-R was much smaller than that in the LTO-R, confirming the lower generation of oxygen vacancies (V_O). The order of white line intensity (LTO-O $\approx$ Mo-LTO-R $>$ LTO-R) at about 4990 eV, formed by the $1s \rightarrow 4p$ allowed transition, was exactly opposite to that of the pre-edge intensity, which was because the higher *p*–*d* hybridization led to a lower probability of the $1s \rightarrow 4p$ transition[9].

Ti *K*-edge EXAFS studies were carried out in order to understand the fine structure variation in more detail (Figure 3 (b)) (further details regarding the EXAFS data processing procedure, and the data fitting to the FEFF model, can be found in Figure S3 and Table S2, respectively). The results of the EXAFS analysis, in particular the Debye–Waller factors given in Table S2, confirmed that the distortion of the TiO_6 octahedral structure in LTO-R was the highest among all the samples, with that of Mo-LTO-R being quite close to that of LTO-O.

It is widely recognized that an increase in structural disorder can result in a decrease in Li ion mobility[26]. Hence, we performed galvanostatic intermittent titration technique (GITT) measurements in order to experimentally determine the ionic mobility (Figure S4). As expected, the lowest ionic mobility was found for LTO-R, while the highest was for Mo-LTO-R. While it is known that the lattice parameter and particle size can affect ionic mobility, as all the samples tested displayed similar values for these (Figure S1 and Table S1), it was deduced that the main factor affecting the ionic mobility was the distortion of the TiO_6 octahedral structure. In summary, thermal treatment in the reducing atmosphere resulted in a decrease in ionic mobility, but an also enhanced electronic conductivity, while Mo doping under the same conditions led to a marked increase in both electronic conductivity and ionic mobility.

Finally, we carried out battery performance tests for the three different materials. In the charge/discharge profile, where the cut-off voltage range was 1–3 V (vs. Li^+/Li), the lowest voltage difference at 1.5 V between the charge and discharge processes was found for Mo-LTO-R, indicating a decrease in polarization caused by the increase in electronic conductivity (Figure 4 (a)). In addition, as shown in Figure 4 (b), it is clear that the Mo doping in the reducing atmosphere was a remarkably efficient method for enhancing the rate capability. While all the samples demonstrated a good capacity close to the theoretical value at a low C-rate, a marked capacity decrease was shown for LTO-O and LTO-R at a high C-rate, which was because of low electronic conductivity and low ionic mobility, respectively. On the other hand, it is interesting to note that almost no deterioration in capacity was exhibited by Mo-LTO-R, even at a high C-rate. In particular, the capacity at 10 C reached 167 mAh g^{-1}, which is extremely close to the theoretical value (172 mAh g^{-1} for 3% Mo-doped LTO). To the best of our knowledge, this is the highest capacity among those previously reported for doped LTO. Furthermore, while almost no capacity change was measured for Mo-LTO-R after 5 weeks stored in air, the capacity of LTO-R deteriorated significantly owing to its unstable lattice structure, with a number of oxygen vacancies (V_O) that could be readily re-oxidized in the air. Hence, it can be concluded that Mo doping in a reducing atmosphere is a promising approach to enhancing the performance of LTO as an anode material for use in high power Li ion batteries.

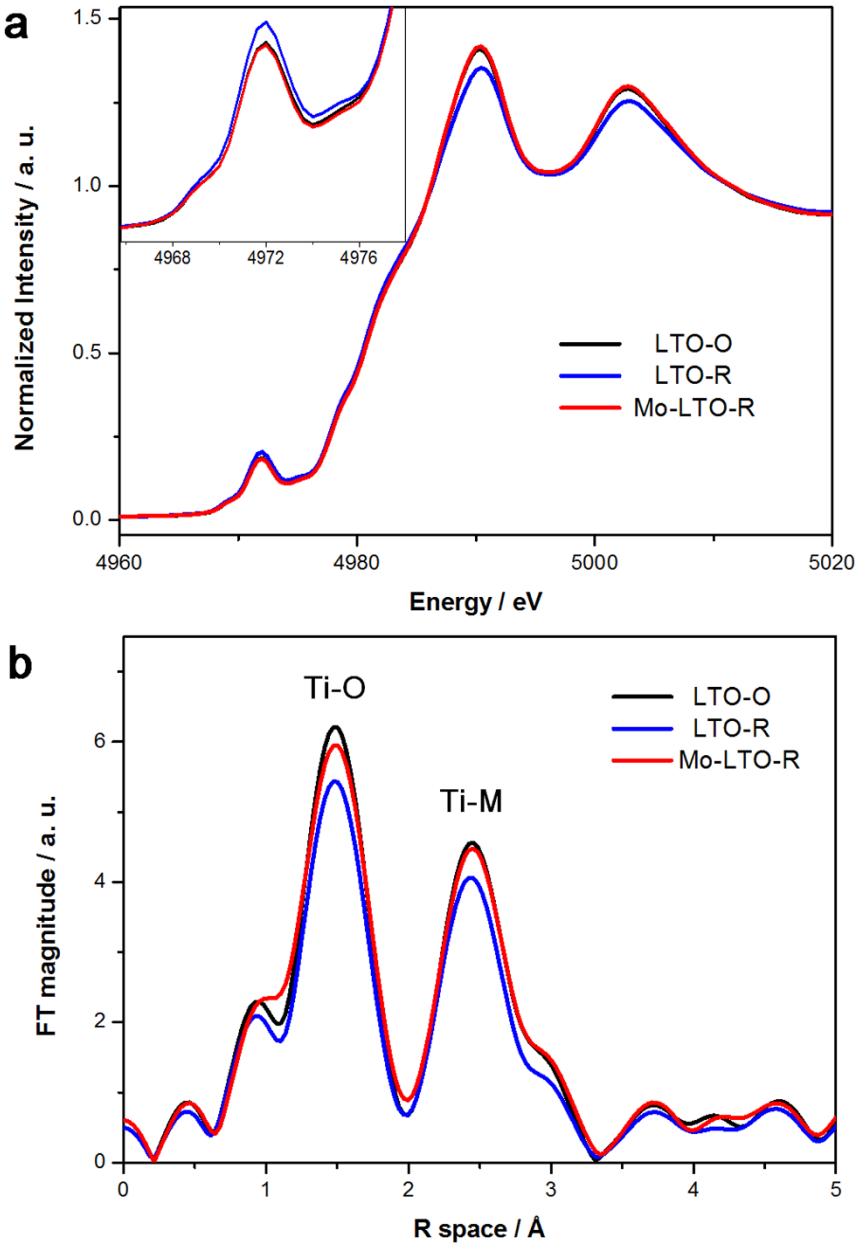

Figure 3 | (a) Ti K-edge XANES spectra and (b) EXAFS spectra of LTO-O, LTO-R, and Mo-LTO-R.

The methodology works by increasing the electronic conductivity, with less generation of oxygen vacancies (V_O), and improving the ionic mobility, with less distortion of the TiO_6 octahedral structure, and simultaneously preserving the structural stability in air.

Several research groups have already reported electrochemical properties of Mo-doped LTO. Yi et al. synthesized Mo-doped LTO by the solid-state method in an oxidizing atmosphere, showing an enhancement of rate capability in the range of 0–2.5 V (vs. Li^+/Li). However, the plateau observed around 1.5 V (vs. Li^+/Li), generated by the redox potential of Ti^{4+}/Ti^{3+}, was shortened by Mo doping, which showed deteriorated battery performance compared to undoped LTO in the voltage range above 1 V (Li^+/Li)[27]. Likewise, our Mo-LTO-O also showed a lower rate capability than the undoped LTO as shown in Figure S5, because Mo was not perfectly doped into LTO but formed an insulating byproduct phase, Li_2MoO_4, which cannot cause an electronic state change of Ti^{4+}. Also, the heat treatment in an oxidizing atmosphere suppresses the oxygen vacancies and thereby cannot contribute to increasing the electronic conductivity[28]. These can be supported by the white color of Mo-LTO-O sample in Figure 1, indicating its insulating characteristic.

Zhang et al. reported the electrochemical performance of Mo-doped LTO annealed in a reducing atmosphere. They suggested that Mo-doping impeded the transportation of Li^+ ions into LTO, thus less amounts of Li^+ ions could be inserted into the LTO structure, which resulted in a decrease in specific capacity at low C-rates[29]. However, in our results, as shown in Figure 4, there was no remarkable difference of capacity between Mo-LTO-R and LTO-O at low C-rates. In our previous work, we reported that the oxidation state of Ti was more prominently changed for the Cr-doped LTO than for the undoped LTO during the Li^+ ions insertion, suggesting that the amounts of inserted Li^+ ions were not affected by doping[9]. Zhang et al. also reported that the generation of Ti^{3+} led to the enhancement of electrochemical performance[29]. However, as mentioned before, the Ti^{3+} state is usually not stable enough in the air as it can be easily oxidized even by dissolved oxygen in water[15], and LTO-R in this study having more amounts of Ti^{3+} than Mo-LTO-R showed the deterioration of battery performance over time due to the increase

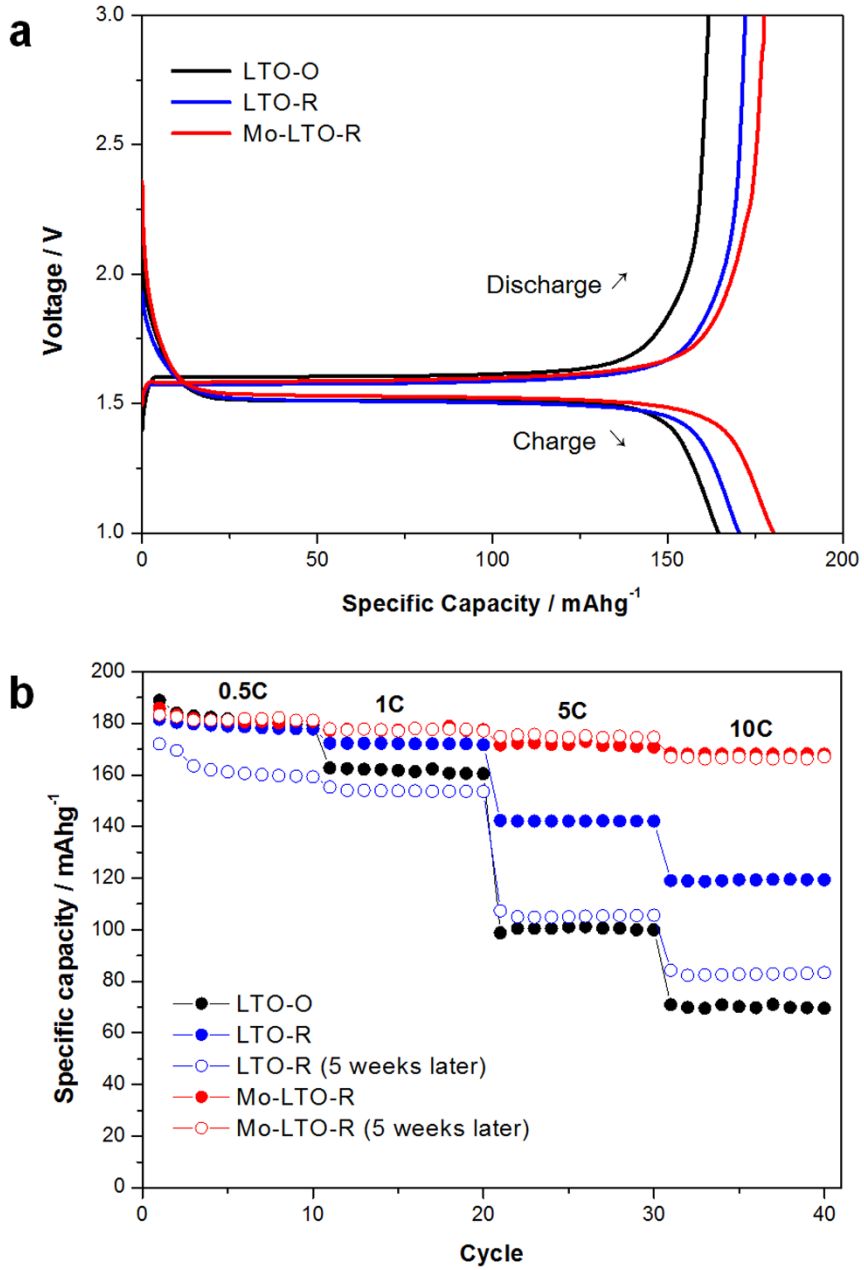

Figure 4 | (a) Charge–discharge profiles at 1 C and (b) rate capability of LTO-O, LTO-R, and Mo-LTO-R.

of structural instability. (Figure 3, 4) Hence, the generation of Ti^{3+} cannot guarantee the enhancement of battery performance. In this study, we were able to find the stabilization of oxygen-deficient LTO by Mo doping due to the delocalized electronic distribution and the markedly enhanced performance as shown in Figure 4.

Discussion

To achieve better understanding of the obtained results, the [110] direction of the lattice structure of each of the prepared materials was constructed (Figure 5). For the LTO-O, all the Ti sites were in the 4+ valence state, with no free electron in Ti d-band, which is the origin of their insulating nature. In addition, there were no structural defects found in the lattice. For LTO-R, a proportion of the Ti sites were in the 3+ valence state, caused by the generation of oxygen vacancies (V_O) during thermal treatment in the reducing atmosphere. This could lead to an increase of electronic conductivity; however, a number of structural defects were inevitably generated. In particular, as identified from the XPS results, the extra charges were localized only in the vicinity of the oxygen vacancies (V_O). As such localized charge distribution is unstable, the improved electron conductivity gradually deteriorated with time and eventually reached a similar level to that of the LTO-O by re-oxidization in air (Table 1). Furthermore, the generation of oxygen vacancies (V_O) resulted in an increase in local disorder of the octahedral structure, as confirmed by XANES and EXAFS analysis (Figure 3), meaning that the Li ion mobility decreased, as identified from the GITT results. On the other hand, in the case of Mo-LTO-R, even though the Ti sites were reduced in a similar manner to LTO-R, and therefore the electronic conductivity was increased, the extra charges were delocalized over all of the Ti sites in the lattice, as confirmed by XPS, which is in contrast to LTO-R. In particular, the quantity of oxygen vacancies (V_O) in the Mo-LTO-R was significantly reduced in comparison with LTO-R, as shown in the EPR results. This is because the delocalization of extra charges generated not by oxygen vacancy formation, but by charge compensation by the high valence Mo dopant, led to the markedly enhanced structural stability, which was much less reactive with

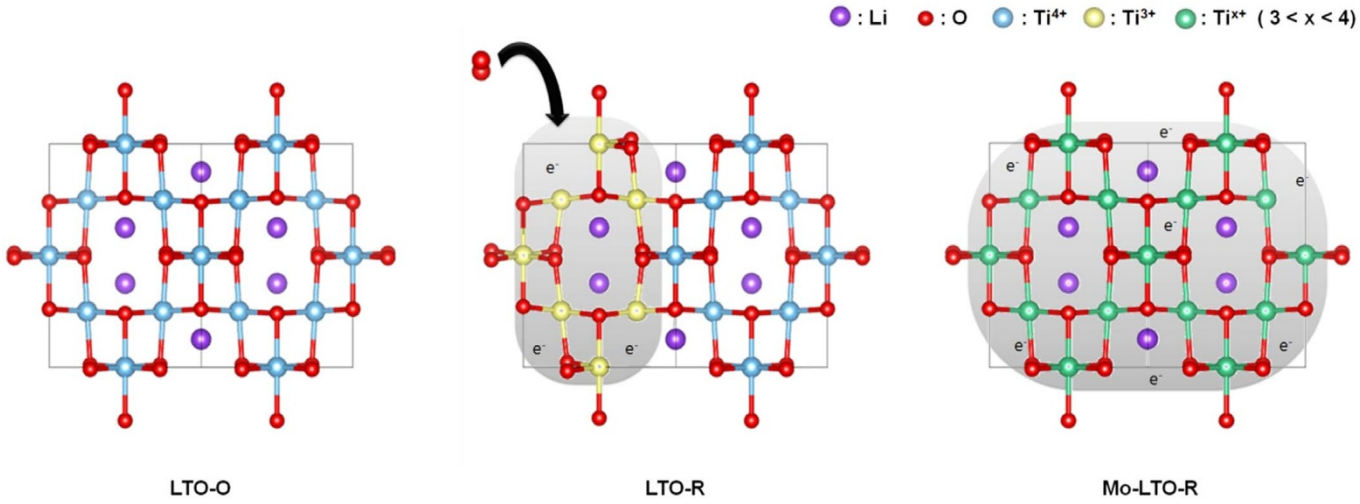

Figure 5 | Estimated structures of LTO-O, LTO-R, and Mo-LTO-R in the [110] direction.

oxygen in the air. Furthermore, since the local disorder of the octahedral structure of Mo-LTO-R was less significant than that of the LTO-R, as identified from the Debye–Waller factors obtained in the EXAFS analysis, no deterioration in Li ion mobility was identified, as confirmed by the GITT results. Hence, the enhanced electronic conductivity and ionic mobility eventually resulted in the greatly enhanced anode performance, particularly at a high C-rate.

In conclusion, we successfully synthesized Mo-doped LTO through simple thermal treatment in a reducing atmosphere. The prepared material demonstrated markedly enhanced electronic conductivity (10^{-2} S cm^{-1}) and rate capability (167 mAh g^{-1} at 10 C) in comparison to the non-doped samples. In particular, the Mo-LTO-R sample did not display any deterioration in anode performance over time, in contrast to the LTO-R, which was due to its structural stability in air being significantly improved by the lower proportion of oxygen vacancies (V_O) generated as a consequence of charge delocalization. Hence, we firmly believe that Mo doping in a reducing atmosphere is a promising approach to addressing the drawbacks of LTO. We expect that the performance of LTO as an anode material could be further enhanced by combining this approach with conventional methods such as nanoscale synthesis and producing composites with conducting materials.

Methods

Synthesis. $Li_4Ti_5O_{12}$ (LTO) and $Li_4Ti_{4.85}Mo_{0.15}O_{12}$ (Mo-LTO) samples were prepared through a conventional solid state method. Mixtures of Li_2CO_3, TiO_2, and MoO_3 with the appropriate molar ratios were milled in liquid ethanol at 50 Hz for 2 h using a ball mill (Mini-Mill PULVERISETTE 23, Fritsch). The obtained slurry was dried and heat treated at 800°C for 5 h at a heating rate of 5°C/min either in air or in a reducing atmosphere (10% H_2 in Ar).

Characterization. The phase compositions and crystal structures of the synthesized powders were characterized using high resolution powder diffraction (HRPD) between 10 and 90° (2θ) at the 9B HRPD beam line of the Pohang light source (PLS).

The electronic conductivities and the mobilities were measured using a Hall effect measurement system (HMS 5000, Ecopia) using the van der Pauw method (four-point probe measurement) with sample powders pressed into pellets at a pressure of 10 ton.

XPS spectra were recorded on a PHI 5000 VersaProbe system using a monochromated Al Kα X-ray beam. Charge correction was performed using the C 1 s peak (284.6 eV) as the reference. Shirley background subtraction was applied to all XPS data. All peaks were fitted with a Gaussian–Lorentzian function to deconvolute overlapping peaks.

X-ray absorption spectroscopy (XAS) of the Ti *K*-edge of the sample powders was carried out in transmission mode at the 10 C Wide-XAFS beam line of the PLS in the 3.0 GeV storage ring with a ring current of 70–100 mA. The background absorption spectrum was subtracted using IFEFFIT software[30], and XANES spectra were obtained by normalization. The k-space range was set to 0.5–11 Å^{-1}, and EXAFS data were obtained by performing a Fourier transform to the r-space. To compensate for damping, the *k*-weight was set to 3, and the interatomic bond length and Debye–Waller factors were obtained by curve fitting performed in the r-range of 1.0–3.4 Å.

Battery tests. The sample electrodes were prepared with active material, acetylene black, and polyvinyl difluoride (PVdF) at a weight ratio of 80 : 10 : 10. The slurry was coated on Cu foil and dried at 75°C in a vacuum for 24 h. A microporous polyethylene membrane was used as a separator, and 1 M $LiPF_6$ in ethylene carbonate (EC) and dimethyl carbonate (DMC) (1 : 1, v/v) was used as the electrolyte. The coin cells (CR2032) were assembled with Li foil on a Cu mesh as the counter and reference electrode in a glove box filled with Ar gas. The charge and discharge tests were carried out on a standard battery cycler (WBCS3000S, WonATech) at different C-rates in the potential range of 1.0–3.0 V (vs Li^+/Li). The diffusion coefficients of the Li ions in all samples were measured using GITT[31].

1. He, Y.-B. *et al.* Gassing in $Li_4Ti_5O_{12}$-based batteries and its remedy. *Sci. Rep.* **2**, 913–921 (2012).
2. Ohzuku, T., Ueda, A. & Yamamoto, N. Zero-Strain Insertion Material of $Li[Li_{1/3}Ti_{5/3}]$ O_4 for Rechargeable Lithium Cells. *J. Electrochem. Soc.* **142**, 1431–1435 (1995).
3. Thackeray, M. M. Structural Considerations of Layered and Spinel Lithiated Oxides for Lithium Ion Batteries. *J. Electrochem. Soc.* **142**, 2558–2563 (1995).
4. Chen, C. H. *et al.* Studies of Mg-substituted $Li_{4-x}Mg_xTi_5O_{12}$ spinel electrodes ($0 \leq x \leq 1$) for lithium batteries. *J. Electrochem. Soc.* **148**, A102–A104 (2001).
5. Feckl, J. M., Fominykh, K., Döblinger, M., Fattakhova-Rohlfing, D. & Bein, T. Nanoscale Porous Framework of Lithium Titanate for Ultrafast Lithium Insertion. *Angew. Chem. Int. Ed.* **51**, 7459–7463 (2012).
6. Ganapathy, S. & Wagemaker, M. Nanosize Storage Properties in Spinel $Li_4Ti_5O_{12}$ Explained by Anisotropic Surface Lithium Insertion. *ACS Nano* **6**, 8702–8712 (2012).
7. Jung, H.-G. *et al.* Microscale spherical carbon-coated $Li_4Ti_5O_{12}$ as ultra high power anode material for lithium batteries. *Energy Environ. Sci.* **4**, 1345–1351 (2011).
8. Zhao, L., Hu, Y.-S., Li, H., Wang, Z. & Chen, L. Porous $Li_4Ti_5O_{12}$ Coated with N-Doped Carbon from Ionic Liquids for Li-Ion Batteries. *Adv. Mater.* **23**, 1385–1388 (2011).
9. Song, H. *et al.* Anomalous decrease in structural disorder due to charge redistribution in Cr-doped $Li_4Ti_5O_{12}$ negative-electrode materials for high-rate Li-ion batteries. *Energy Environ. Sci.* **5**, 9903–9913 (2012).
10. Capsoni, D. *et al.* Cations Distribution and Valence States in Mn-Substituted $Li_4Ti_5O_{12}$ Structure. *Chem. Mater.* **20**, 4291–4298 (2008).
11. Yip, T. W. S., Cussen, E. J. & Wilson, C. Spontaneous formation of crystalline lithium molybdate from solid reagents at room temperature. *Dalton Trans.* **39**, 411–417 (2010).
12. Yuan, T., Cai, R. & Shao, Z. Different Effect of the Atmospheres on the Phase Formation and Performance of $Li_4Ti_5O_{12}$ Prepared from Ball-Milling-Assisted Solid-Phase Reaction with Pristine and Carbon-Precoated TiO_2 as Starting Materials. *J. Phys. Chem. C* **115**, 4943–4952 (2011).
13. Wolfenstine, J., Lee, U. & Allen, J. L. Electrical conductivity and rate-capability of $Li_4Ti_5O_{12}$ as a function of heat-treatment atmosphere. *J. Power Sources* **154**, 287–289 (2006).
14. Shen, L., Uchaker, E., Zhang, X. & Cao, G. Hydrogenated $Li_4Ti_5O_{12}$ Nanowire Arrays for High Rate Lithium Ion Batteries. *Adv. Mater.* **24**, 6502–6506 (2012).
15. Zuo, F., Wang, L., Wu, T., Zhang, Z., Borchardt, D. & Feng, P. Self-Doped Ti^{3+} Enhanced Photocatalyst for Hydrogen Production under Visible Light. *J. Am. Chem. Soc.* **132**, 11856–11857 (2010).

16. Komaguchi, K., Maruoka, T., Nakano, H., Imae, I., Ooyama, Y. & Harima, Y. Electron-Transfer Reaction of Oxygen Species on TiO_2 Nanoparticles Induced by Sub-band-gap Illumination. *J. Phys. Chem. C* **114**, 1240–1245 (2009).
17. Shin, J.-Y., Joo, J. H., Samuelis, D. & Maier, J. Oxygen-Deficient $TiO_{2-\delta}$ Nanoparticles via Hydrogen Reduction for High Rate Capability Lithium Batteries. *Chem. Mater.* **24**, 543–551 (2011).
18. Ressler, T., Jentoft, R. E., Wienold, J., Gunter, M. M. & Timpe, O. In Situ XAS and XRD Studies on the Formation of Mo Suboxides during Reduction of MoO_3. *J. Phys. Chem. B* **104**, 6360–6370 (2000).
19. Guittet, M. J., Crocombette, J. P. & Gautier-Soyer, M. Bonding and XPS chemical shifts in $ZrSiO_4$ versus SiO_2 and ZrO_2:Charge transfer and electrostatic effects. *Phys. Rev. B* **63**, 125117–125123 (2001).
20. Demadis, K. D., Hartshorn, C. M. & Meyer, T. J. The Localized-to-Delocalized Transition in Mixed-Valence Chemistry. *Chem. Rev.* **101**, 2655–2686 (2001).
21. Matsumoto, K. *et al.* Syntheses and Crystal Structures of Disulfide-Bridged Binuclear Ruthenium Compounds: The First UV−Vis, Raman, ESR, and XPS Spectroscopic Characterization of a Valence-Averaged Mixed-Valent $Ru^{III}SSRu^{II}$ Core. *J. Am. Chem. Soc.* **118**, 3597–3609 (1996).
22. Hoang, S., Berglund, S. P., Hahn, N. T., Bard, A. J. & Mullins, C. B. Enhancing Visible Light Photo-oxidation of Water with TiO_2 Nanowire Arrays via Cotreatment with H_2 and NH_3: Synergistic Effects between Ti^{3+} and N. *J. Am. Chem. Soc.* **134**, 3659–3662 (2012).
23. Lindan, P. J. D., Harrison, N. M., Gillan, M. J. & White, J. A. First-principles spin-polarized calculations on the reduced and reconstructed TiO_2 (110) surface. *Phys. Rev. B* **55**, 15919–15927 (1997).
24. Jiang, N., Su, D. & Spence, J. C. H. Determination of Ti coordination from pre-edge peaks in Ti K -edge XANES. *Phys. Rev. B* **76**, 214117–214125 (2007).
25. Kim, D., Hong, J., Park, Y. R. & Kim, K. J. The origin of oxygen vacancy induced ferromagnetism in undoped TiO_2. *J. Phys.: Condens. Matter* **21**, 195405–195408 (2009).
26. Ariyoshi, K., Yamato, R. & Ohzuku, T. Zero-strain insertion mechanism of $Li[Li_{1/3}Ti_{5/3}]O_4$ for advanced lithium-ion (shuttlecock) batteries. *Electrochim. Acta* **51**, 1125–1129 (2005).
27. Yi, T.-F. *et al.* Advanced electrochemical properties of Mo-doped $Li_4Ti_5O_{12}$ anode material for power lithium ion battery. *RSC Adv.* **2**, 3541–3547 (2012).
28. Khare, N., Kappers, M. J., Wei, M., Blamire, M. G. & MacManus-Driscoll, J. L. Defect-Induced Ferromagnetism in Co-doped ZnO. *Adv. Mater.* **18**, 1449–1452 (2006).
29. Zhang, X.-L., Hu, G.-R. & Peng, Z.-D. Preparation and Effects of Mo-doping on the Electrochemical Properties of Spinel $Li_4Ti_5O_{12}$ as Anode Material for Lithium Ion Battery. *Journal of Inorganic Materials* **26**, 443 (2011).
30. Ravel, B. & Newville, M. ATHENA, ARTEMIS, HEPHAESTUS: data analysis for X-ray absorption spectroscopy using IFEFFIT. *J. Synchrotron Radiat.* **12**, 537–541 (2005).
31. Weppner, W. & Huggins, R. A. Determination of the Kinetic Parameters of Mixed-Conducting Electrodes and Application to the System Li_3Sb. *J. Electrochem. Soc.* **124**, 1569–1578 (1977).

Acknowledgments

This work was supported by a National Research Foundation of Korea (NRF) grant funded by the Korean government (MEST) (NRF-2011-C1AAA001-0030538, NRF-2012R1A1A2007624, 2012-0008830, GCRC-SOP).

Author contributions

H.S. and Y.-T.K. proposed the concept and H.S. performed the experiment. T.-G.J., Y.H.M., H.-H.C., K.Y.C., H.S.K. and B.W.C. participated in acquiring the data. H.S. and Y.-T.K. wrote the paper. All authors commented on the paper.

Additional information

Supplementary information accompanies this paper at http://www.nature.com/scientificreports

Competing financial interests: The authors declare no competing financial interests.

How to cite this article: Song, H. *et al.* Stabilization of Oxygen-deficient Structure for Conducting $Li_4Ti_5O_{12-\delta}$ by Molybdenum Doping in a Reducing Atmosphere. *Sci. Rep.* **4**, 4350; DOI:10.1038/srep04350 (2014).